

Study of Particle Production in Quark vs. Gluon Fragmentation at $\sqrt{s} \sim 10 \text{ GeV}^*$

R. A. Briere,¹ I. Brock,¹ J. Chen,¹ T. Ferguson,¹ G. Tatishvili,¹ H. Vogel,¹ M. E. Watkins,¹
 J. L. Rosner,² N. E. Adam,³ J. P. Alexander,³ K. Berkelman,³ D. G. Cassel,³
 J. E. Duboscq,³ K. M. Ecklund,³ R. Ehrlich,³ L. Fields,³ R. S. Galik,³ L. Gibbons,³
 R. Gray,³ S. W. Gray,³ D. L. Hartill,³ B. K. Heltsley,³ D. Hertz,³ C. D. Jones,³
 J. Kandaswamy,³ D. L. Kreinick,³ V. E. Kuznetsov,³ H. Mahlke-Krüger,³ P. U. E. Onyisi,³
 J. R. Patterson,³ D. Peterson,³ J. Pivarski,³ D. Riley,³ A. Ryd,³ A. J. Sadoff,³
 H. Schwarthoff,³ X. Shi,³ S. Stroiney,³ W. M. Sun,³ T. Wilksen,³ M. Weinberger,³
 S. B. Athar,⁴ R. Patel,⁴ V. Potlia,⁴ J. Yelton,⁴ P. Rubin,⁵ C. Cawfield,⁶ B. I. Eisenstein,⁶
 I. Karliner,⁶ D. Kim,⁶ N. Lowrey,⁶ P. Naik,⁶ C. Sedlack,⁶ M. Selen,⁶ E. J. White,⁶
 J. Wiss,⁶ M. R. Shepherd,⁷ D. Besson,⁸ H. K. Swift,⁸ T. K. Pedlar,⁹ D. Cronin-Hennessy,¹⁰
 K. Y. Gao,¹⁰ D. T. Gong,¹⁰ J. Hietala,¹⁰ Y. Kubota,¹⁰ T. Klein,¹⁰ B. W. Lang,¹⁰
 R. Poling,¹⁰ A. W. Scott,¹⁰ A. Smith,¹⁰ P. Zweber,¹⁰ S. Dobbs,¹¹ Z. Metreveli,¹¹
 K. K. Seth,¹¹ A. Tomaradze,¹¹ J. Ernst,¹² H. Severini,¹³ S. A. Dytman,¹⁴ W. Love,¹⁴
 V. Savinov,¹⁴ O. Aquines,¹⁵ Z. Li,¹⁵ A. Lopez,¹⁵ S. Mehrabyan,¹⁵ H. Mendez,¹⁵
 J. Ramirez,¹⁵ G. S. Huang,¹⁶ D. H. Miller,¹⁶ V. Pavlunin,¹⁶ B. Sanghi,¹⁶ I. P. J. Shipsey,¹⁶
 B. Xin,¹⁶ G. S. Adams,¹⁷ M. Anderson,¹⁷ J. P. Cummings,¹⁷ I. Danko,¹⁷ J. Napolitano,¹⁷
 Q. He,¹⁸ J. Insler,¹⁸ H. Muramatsu,¹⁸ C. S. Park,¹⁸ E. H. Thorndike,¹⁸ F. Yang,¹⁸
 T. E. Coan,¹⁹ Y. S. Gao,¹⁹ F. Liu,¹⁹ M. Artuso,²⁰ S. Blusk,²⁰ J. Butt,²⁰ J. Li,²⁰ N. Menaa,²⁰
 G. C. Moneti,²⁰ R. Mountain,²⁰ S. Nisar,²⁰ K. Randrianarivony,²⁰ R. Redjimi,²⁰ R. Sia,²⁰
 T. Skwarnicki,²⁰ S. Stone,²⁰ J. C. Wang,²⁰ K. Zhang,²⁰ S. E. Csorna,²¹ G. Bonvicini,²²
 D. Cinabro,²² M. Dubrovin,²² A. Lincoln,²² D. M. Asner,²³ and K. W. Edwards²³

(CLEO Collaboration)

¹*Carnegie Mellon University, Pittsburgh, Pennsylvania 15213*

²*Enrico Fermi Institute, University of Chicago, Chicago, Illinois 60637*

³*Cornell University, Ithaca, New York 14853*

⁴*University of Florida, Gainesville, Florida 32611*

⁵*George Mason University, Fairfax, Virginia 22030*

⁶*University of Illinois, Urbana-Champaign, Illinois 61801*

⁷*Indiana University, Bloomington, Indiana 47405*

⁸*University of Kansas, Lawrence, Kansas 66045*

⁹*Luther College, Decorah, Iowa 52101*

¹⁰*University of Minnesota, Minneapolis, Minnesota 55455*

¹¹*Northwestern University, Evanston, Illinois 60208*

¹²*State University of New York at Albany, Albany, New York 12222*

¹³*University of Oklahoma, Norman, Oklahoma 73019*

¹⁴*University of Pittsburgh, Pittsburgh, Pennsylvania 15260*

¹⁵*University of Puerto Rico, Mayaguez, Puerto Rico 00681*

¹⁶*Purdue University, West Lafayette, Indiana 47907*

¹⁷*Rensselaer Polytechnic Institute, Troy, New York 12180*

¹⁸*University of Rochester, Rochester, New York 14627*

¹⁹*Southern Methodist University, Dallas, Texas 75275*

²⁰*Syracuse University, Syracuse, New York 13244*

²¹*Vanderbilt University, Nashville, Tennessee 37235*

²²*Wayne State University, Detroit, Michigan 48202*

²³*Carleton University, Ottawa, Ontario, Canada K1S 5B6*

Abstract

Using data collected with the CLEO III detector at the Cornell Electron Storage Ring, we have compared proton, lambda (charged conjugate modes are implicit) and meson (ϕ and $f_2(1270)$) production observed in gluon fragmentation vs. quark fragmentation. Two studies have been conducted: in the first, we corroborate previous per-event particle yields in $\Upsilon \rightarrow ggg$ vs. $e^+e^- \rightarrow q\bar{q}$. In the second, we compare particle production in the photon-tagged process $\Upsilon(1S) \rightarrow gg\gamma$ with that in $e^+e^- \rightarrow q\bar{q}\gamma$ events. For each particle, we determine the ‘enhancement’ ratio, defined as the ratio of particle yields per gluon fragmentation event compared to quark fragmentation event. Thus defined, an enhancement of 1.0 implies equal per-event production in both gluon and quark fragmentation. In the photon-tagged analysis, we find an enhancement of order unity for protons and approximately 1.5 for Λ 's. This measured proton enhancement rate is supported by a study of baryon production in $\chi_{b,2} \rightarrow p + X$ relative to $\chi_{b,1} \rightarrow p + X$. The production of mesons having masses of order 1 GeV (ϕ and $f_2(1270)$) are found to be also approximately the same in $gg\gamma$ vs. $q\bar{q}\gamma$ fragmentation. Overall, per-event baryon production in two-gluon fragmentation is considerably smaller than that observed in three-gluon decays of the $\Upsilon(1S)$. Our results for baryon production are inconsistent with the predictions of the JETSET (7.4) fragmentation model. The results presented in this document are preliminary.

*Submitted to the 33rd International Conference on High Energy Physics, July 26 - August 2, 2006, Moscow

I. INTRODUCTION

Understanding hadronization, or the process by which elementary partons (gluons and quarks) evolve into mesons and baryons, is complicated by its intrinsically non-perturbative nature. Due to the fact that gluons carry two color indices whereas quarks carry only one, the intrinsic gluon-gluon coupling strength ($C_A=3$) is larger than the intrinsic quark-gluon coupling strength ($C_F=4/3$). Radiation of secondary and tertiary gluons is therefore expected to be more likely when hadronization is initiated by a gluon rather than by a quark. This results in a greater number of final state hadrons as well as a larger average transverse momentum in the former case compared to the latter case. In the limit $Q^2 \rightarrow \infty$, the ratio of the number of hadrons produced in gluon-initiated jets to the number of hadrons produced in quark-initiated jets is expected, in lowest order, to approach the well-known color-counting ratio $C_A/C_F=9/4$ [1].

Many experiments have searched for, and found, multiplicity and jet shape differences between quark and gluon fragmentation. At Z^0 energies, $q\bar{q}g$ events are distinguished by their three-jet topology. Within such events, quark and gluon jets can be separated by a variety of techniques including vertex tagging. Because gluons rarely fragment into heavy quarks, they will produce jets that form a vertex at the e^+e^- interaction point. Quark jets, to the contrary, tend to form a detached vertex when the jet contains a long-lived bottom or charm quark. For light-quark events with gluon radiation, however, the assignment of final state hadrons to the initial state partons is generally more ambiguous and often relies on Monte Carlo simulations to determine the fraction of times that an observed hadron is correctly traced to a primary parton.

Within the limits of their precision, previous studies at SLD found inclusive production of pions, kaons and protons to be equivalent for gluon-tagged and quark-tagged jets[2]. OPAL has measured charm production at the level of $(3.20 \pm 0.21 \pm 0.38)\%$ in gluon jets[3, 4], more than an order of magnitude smaller than the rate observed in quark jets at the Z^0 . ALEPH[5] and DELPHI[6] both measured inclusive bottom production in gluon-tagged jets to be $2 - 3 \times 10^{-3}$, again considerably smaller than that expected from charge counting in quark fragmentation. Most directly comparable to our current work, OPAL has also compared inclusive K_s^0 and Λ production in gluon- vs. quark-tagged jets, finding inclusive production ratios again consistent with unity ($0.94 \pm 0.07 \pm 0.07$ and $1.18 \pm 0.01 \pm 0.17$, respectively)[7].

The 10 GeV center of mass energy range offers a unique opportunity to probe quark and gluon fragmentation effects, without relying on Monte Carlo simulation to associate the final state hadrons with an initial state parton. The decay $\Upsilon(1S) \rightarrow gg\gamma$ allows one to compare the gg system in a $gg\gamma$ event with the $q\bar{q}$ system in $e^+e^- \rightarrow q\bar{q}\gamma$ events. In both cases, the system recoiling against the photon consists (to lowest order) of hadrons that have evolved from either a two-gluon or a quark-antiquark system. The properties of the recoil systems can then be compared directly.¹ Additionally, the radiative transitions from the radially excited Υ states to the orbitally excited χ_b triplet offers an opportunity to further

¹ Although there may be gluon radiation from the initial partons, we do not distinguish such radiation explicitly in this analysis. Thus, the states that we are comparing are, strictly speaking, $gg\gamma$ and $q\bar{q}\gamma$ to lowest-order only; additional gluon radiation, to which we are not experimentally sensitive, may be present in many of the events in our sample. Without the ability to adequately identify additional gluons, such higher-order radiative effects are therefore implicitly absorbed into the experimental measurement.

probe fragmentation differences between decays of the $J=0$ and $J=2$ χ_b states (decaying predominantly to two gluons) vs. decays of the $J=1$ state (decaying primarily to $q\bar{q}(g)$ final states, with the gluon nearly on-shell). Statistical correlations between transition photons with inclusive production of particular final-state particles (X) allows a measurement of the relative yields of $gg \rightarrow X:q\bar{q}(g) \rightarrow X$.

In this analysis, we focus on the relative production rates of baryons (protons and Λ 's) and heavy mesons (ϕ and $f_2(1270)$) in gluon vs. quark fragmentation (charge conjugation is implied). A previous study noted apparent enhancements in the production of ϕ , Λ and protons in three-gluon decays of the $\Upsilon(1S)$ [8], albeit with low statistics and at no more than $2-3\sigma$ significance. That initial study also found approximately one unit larger charged multiplicity for three-gluon fragmentation of the $\Upsilon(1S)$ compared to $q\bar{q}$ fragmentation at a comparable center-of-mass energy. With the limited statistics at that time, the additional unit of multiplicity could entirely be accounted for by enhanced three-gluonic production of baryons. We now have sufficient statistics to re-measure the three-gluon particle production rates, and also to compare, for the first time, inclusive production in two-gluon fragmentation vs. inclusive production in three-gluon fragmentation.

Since then, other experimental data on quark/gluon fragmentation differences in the $\sqrt{s} \sim 10$ GeV energy regime have become available, including (per event):

1. A suppression of production of open charm in gluonic decays of the Υ resonances: $(\Upsilon(1S) \rightarrow ggg \rightarrow D + X)/(e^+e^- \rightarrow D + X) \sim 0.02$ [9].
2. The observation that fragmentation of the $J=1$ state of the χ_b triplet (decaying to $q\bar{q}g$) results in charm production comparable to the underlying continuum; no such charm production is observed in the two-gluon decays of the $J=0$ or $J=2$ states[10].
3. An enhancement in production of hidden charm in gluonic decays of the Υ resonances: $(\Upsilon(1S) \rightarrow ggg \rightarrow J/\psi + X)/(e^+e^- \rightarrow J/\psi + X) > 5.3$ [11].
4. Production of deuterons from resonant 3-gluon decays of both the $\Upsilon(1S)$ and $\Upsilon(2S)$ at the level of 10^{-3} ; no corresponding production of deuterons is observed from the continuum[12]. Per event enhancements are ≥ 10 .
5. Approximately equal production of η' in gluonic decays of the Υ resonance compared to Υ decays via $q\bar{q}$: $(\Upsilon(1S) \rightarrow ggg \rightarrow \eta' + X)/(\Upsilon \rightarrow q\bar{q} \rightarrow \eta' + X) \sim 2/3$, integrated over momentum[13].

II. DETECTOR AND DATA SAMPLE

The CLEO III detector[14, 15] is a general purpose solenoidal magnet spectrometer and calorimeter. This system is very efficient ($\epsilon \geq 98\%$) for detecting tracks that have transverse momenta (p_T) relative to the beam axis greater than 200 MeV/c, and that are contained within the good fiducial volume of the drift chamber ($|\cos\theta| < 0.94$, with θ defined as the polar angle relative to the beam axis). Below this threshold, the charged particle detection efficiency in the fiducial volume decreases to approximately 90% at $p_T \sim 100$ MeV/c. For $p_T < 100$ MeV/c, the efficiency decreases roughly linearly to zero at a threshold of $p_T \approx 30$ MeV/c. Just within the solenoidal magnet coil is the electromagnetic calorimeter, consisting

of 7800 thallium doped CsI crystals. The central “barrel” region of the calorimeter covers about 75% of the solid angle and has an energy resolution of

$$\frac{\sigma_E}{E}(\%) = \frac{0.6}{E^{0.73}} + 1.14 - 0.01E, \quad (1)$$

where E is the shower energy in GeV. This parameterization translates to an energy resolution of about 2% at 2 GeV and 1.2% at 5 GeV. Two end-cap regions of the crystal calorimeter extend solid angle coverage to about 95% of 4π , although energy resolution is not as good as that of the barrel region. The tracking system, RICH particle identification system and calorimeter are all contained within the 1.5 Tesla superconducting coil. Flux return and tracking chambers used for muon detection are located immediately outside the coil and in the two end-cap regions.

We use the CLEO-III data collected at the narrow Υ resonances as a source of $gg\gamma$ events and data taken just below the resonances, as well as the below-4S continuum ($\sqrt{s}=10.55$ GeV) as a source of $q\bar{q}\gamma$ events. The γ in our $q\bar{q}\gamma$ sample results primarily from initial state radiation (ISR)[16]. We compare events for which the fractional photon energy $x_\gamma = E_\gamma/E_{beam}$ are the same.²

A. Data Samples Used and Event Selection

We use data taken at the $\Upsilon(1S)$, $\Upsilon(2S)$, $\Upsilon(3S)$, and $\Upsilon(4S)$ resonances.

We impose event selection requirements identical to those used in our previous study of inclusive direct photon production in Υ decays[17]. Those cuts are designed primarily to suppress backgrounds such as two-photon collisions, QED events (including tau pairs), and beam-gas and beam-wall collisions.

Luminosity, event count, and photon yields ($x_\gamma > 0.5$) are given in Table I.

B. Event Backgrounds

To determine the characteristics of resonant $gg\gamma$ events, we must subtract the background arising from non-resonant $q\bar{q}\gamma$ and $e^+e^- \rightarrow \tau\tau\gamma$ events produced in continuum e^+e^- annihilations at $\sqrt{s} = M_{\Upsilon(1S)}$. This is done by direct scaling of the event samples collected off-resonance on the nearby continuum.

In order to isolate continuum $q\bar{q}\gamma$ events, $\tau\tau\gamma$ contamination must be explicitly subtracted, using a Monte Carlo simulation of tau pair events. We find that $\tau\tau\gamma$ events comprise about 5% of the $q\bar{q}\gamma$ data sample passing the event selection cuts[17]. Beam gas and two photon backgrounds were investigated and found to be negligibly small. The photon-tagged sample can also be contaminated by cases where the high-energy photon is actually a π^0 daughter. Figure 1 illustrates the fraction of photons for the on-1S resonance and below-4S continuum, respectively, that are produced from neutral decays (including not only π^0 decays but also η , η' , and ω decays) as determined from Monte Carlo simulations.

² This deviates from the previous convention, for which the scaling variable was the invariant mass of the gg and $q\bar{q}$ systems recoiling against the hard photon (M_{recoil} , defined by $M_{recoil} = \sqrt{4E_{beam}^2(1 - E_\gamma/E_{beam})}$). We take the difference between results using these two conventions as a systematic error.

TABLE I: Summary of data used in analysis. For each data set, we track the number of photons per unit luminosity, as well as the total number of observed hadronic events per unit luminosity. HadEvs denotes the total number of events in each sample identified as hadronic by our event selection requirements. The number of photons having scaled momentum (relative to E_{beam}) greater than 0.5 is presented in the last column.

DataSet	Type	Resonance	\mathcal{L} (pb^{-1})	HadEvs	$N_\gamma(x > 0.5)$
1S	Data	$\Upsilon(1S)$	1220	22780000	219000
2S	Data	$\Upsilon(2S)$	1070	9450000	88800
3S	Data	$\Upsilon(3S)$	1420	8890000	79500
4S	Data	$\Upsilon(3S)$	5520	18970000	165000
1S-CO	Data	$< \Upsilon(1S)$	144	515000	5700
2S-CO	Data	$< \Upsilon(2S)$	312	932000	10300
3S-CO	Data	$< \Upsilon(3S)$	185	532000	5900
4S-CO	Data	$< \Upsilon(4S)$	2100	5680000	64700
1S	JETSET MC	$\Upsilon(1S)$		1160000	9900
2S	JETSET MC	$\Upsilon(2S)$		9190000	70000
3S	JETSET MC	$\Upsilon(3S)$		3890000	27000
4S	$B\bar{B}$ MC	$\Upsilon(4S)$		8350000	300
1S-CO	JETSET MC	$< \Upsilon(1S)$		8170000	68100
2S-CO	JETSET MC	$< \Upsilon(2S)$		7610000	66600
3S-CO	JETSET MC	$< \Upsilon(3S)$		12850000	115000
4S-CO	JETSET MC	$< \Upsilon(4S)$		63630000	568000

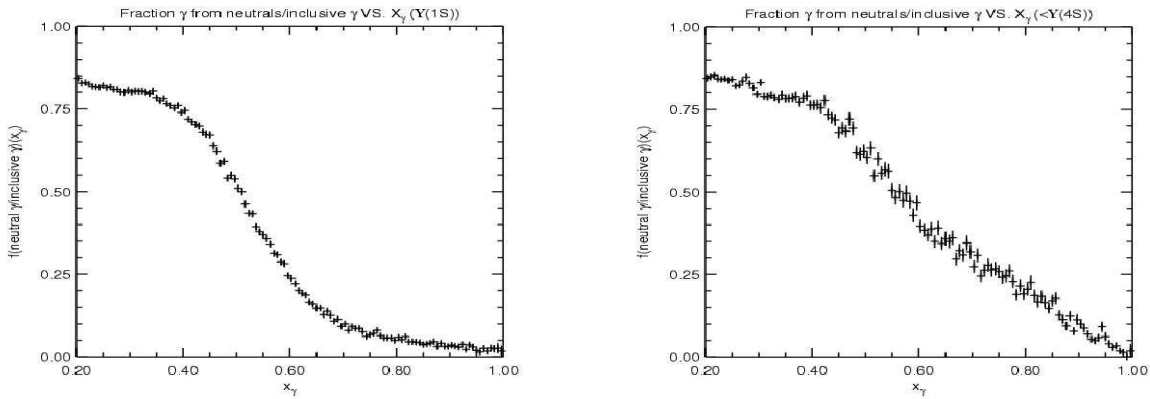


FIG. 1: Monte Carlo prediction for fraction of photons produced by neutral decays (such as π^0 , η , η' , and ω) on the 1S resonance (left) and on the continuum below the 4S resonance (right).

Integrated over all tag photon momenta, π^0 contamination comprises a $\sim 15\%$ background to the direct-photon sample. Monte Carlo simulations also indicate that the π^0 contamination tends to cancel when we take ratios of resonant photon production to continuum photon production.

1. Particle Identification

Our photon and particle identification procedures are identical to those developed in [17]. Photon candidates are selected from showers with widths and patterns of energy deposition consistent with that of a photon, as opposed to neutral hadrons (e.g. merged π^0 's, K_L^0 , neutrons, etc.). To ensure that the events are well-contained within the CLEO detector, we require $|\cos\theta_\gamma| < 0.707$ (θ_γ defined as before as the polar angle between the beam axis and the direct photon). For protons (and antiprotons), we require that charged tracks have specific ionization and also RICH information consistent with that expected for true protons. For momenta less than 1 GeV/c, we require that the track particle identification information be inconsistent (at the level of 2σ) with that expected for true pions. We also require that the proton momentum be greater than 400 MeV, so as to suppress beam-wall and fake backgrounds. For reconstruction of ϕ (and $f_2(1270)$) from kaons (and pions) we require that pairs of opposite charge have particle identification information consistent with their assumed identities. For the case of the f_2 , we require the pion energy to be greater than 500 MeV, to enhance the signal to noise ratio. Lambdas are identified using the standard CLEO algorithms for reconstruction of detached vertices.

2. Backgrounds to the Proton Sample

We use Monte Carlo simulations to assess fake proton backgrounds. Figure 2 illustrates proton fakes for a sample of below-1S Monte Carlo continuum simulations. The solid black curve shows the number of all particles identified as protons that were also tagged as true protons. The red dashed (blue dotted, magenta dash-dot) curve corresponds to those particles that were identified as protons, but that were tagged at the generator level as true kaons (pions, positrons). Proton backgrounds are observed to be present at the $\sim 10\%$ level and are expected to largely cancel in the ratio of ratios.

Note that, for all proton and antiproton identification, we require that the minimum (anti-)proton momentum exceed 400 MeV to eliminate concerns regarding protons ranging out in the beampipe.

C. Signal Definition

In this analysis we measure particle enhancements in both the ggg and $gg\gamma$ decays of the Upsilon system, relative to $q\bar{q}(\gamma)$ production on the underlying continuum. Our definition of enhancement is given quantitatively as the continuum-subtracted resonance yield relative to the continuum yield. Thus defined, an enhancement of 1 indicates that a given particle is produced as often (per event) on the continuum as on the resonance. Note that our definition of ‘continuum’ here means both below-resonance continuum, as well as resonance $\rightarrow q\bar{q}$ through vacuum-polarization; i.e., all $e^+e^- \rightarrow q\bar{q}$ -like processes which must be explicitly subtracted

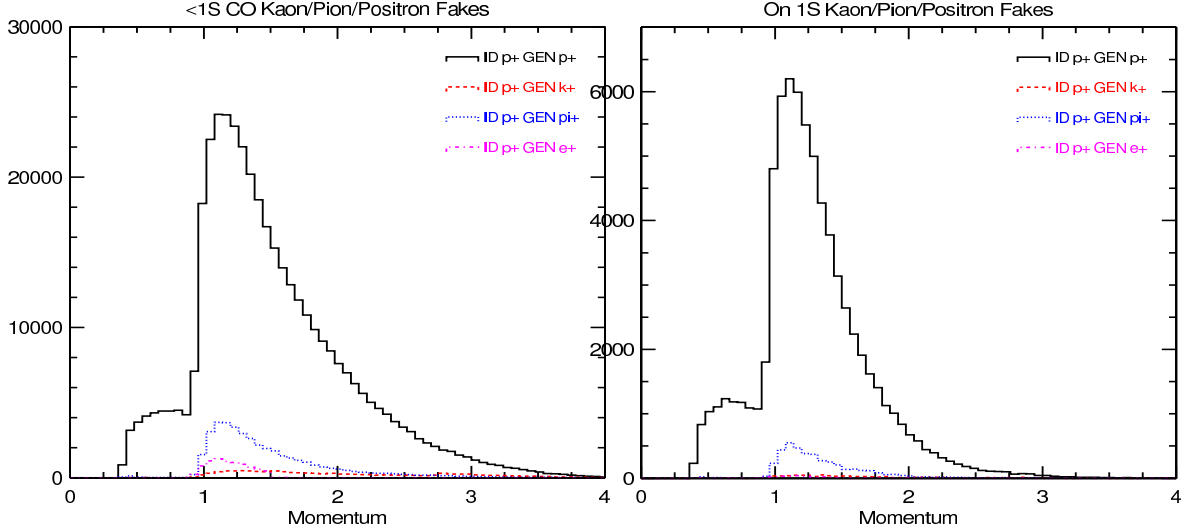


FIG. 2: (Left) Proton fakes for a sample of below-1S Monte Carlo simulations. The solid black curve shows the number of all particles identified as protons that were also tagged as true protons. The red dashed (blue dotted, magenta dash-dot) curve corresponds to those particles that were identified as protons, but that were actually kaons (pions, positrons). (Right) Same for on-1S event simulations.

in determining the characteristics of 3-gluon resonant decays.³ Furthermore, note that for the $\Upsilon(2S)$ and $\Upsilon(3S)$ data, there is no subtraction of cascades to lower Υ states or χ_b decays. Therefore, in what follows, “ $\Upsilon(2S)$ ” denotes a sum over $\Upsilon(2S)$ direct, $\Upsilon(2S) \rightarrow \Upsilon(1S)+X$ and $\Upsilon(2S) \rightarrow \chi_b$. Assuming the direct decays of the Υ resonances are identical, an $\Upsilon(2S)$ enhancement smaller than that of the $\Upsilon(1S)$ implies that the enhancements from the first and third processes enumerated above are therefore smaller than for the $\Upsilon(1S)$.

In general we have two continuum-subtraction options: we may determine enhancements for all resonances relative to the below-4S continuum (for which the statistics are largest, but the extrapolation in energy and run period is also largest) or we may find enhancements relative to their individual below-resonant continua using data not more than 50 MeV away from the resonance of interest. For mass-fitted particles we normalize exclusively to the below-4S continuum, as the individual continua (below-1S, -2S, and -3S) do not have high enough statistics to yield well-fitted mass peaks. For particle counts determined by the momentum spectra (protons and antiprotons), we normalize to both the below-4S continuum as well as the resonance-specific continua and present the differences in the enhancements produced by the two as a systematic error.

³ Vacuum polarization processes are subtracted by direct scaling of the continuum using the $\Upsilon \rightarrow \gamma^* \rightarrow q\bar{q}$ values tabulated previously[17].

D. Particle production in three-gluon vs. $q\bar{q}$ events

The previous CLEO-I analysis already observed significant enhancements of protons and lambda's produced in 3-gluon decays of the 1S relative to the below-4S continuum[8]. We repeat that analysis with our enlarged data set, as described below.

Errors on particle yields are obtained from the error on the fit if the particle count is obtained by fitting a mass peak (Λ, ϕ, f_2) or by the square root of the total count if the particle count is obtained from the momentum spectrum (p, \bar{p}). For the ggg analysis, we determine enhancements as a function of scaled momentum and also calculate momentum-integrated enhancements for each particle, to allow comparison with previous results.

E. $gg\gamma$ Analysis

For the $gg\gamma$ analysis we normalize the particle counts in a given bin to the photon counts in the same bin. In this case the bins are determined by the photon momentum and not the particle momentum (as is the case in the ggg analysis). For each bin, we then find the fractional contamination of resonance photons due to the underlying continuum. Once this fractional contamination is known, the resonance yield can be extracted by straight-forward algebra. As a check of the numerical procedure, we have verified that the enhancements obtained for $\Upsilon(4S)$ (which should produce no photons with $x_\gamma > 0.5$, since its width is dominated by $B\bar{B}$) relative to the below-4S continuum are consistent with zero.

$$Fraction_{Continuum} = \frac{\sigma_{x_\gamma > 0.5}^{Continuum}}{\sigma_{x_\gamma > 0.5}^{Resonance}} \left(\frac{E_{beam}^{Continuum}}{E_{beam}^{Resonance}} \right)^2 \quad (2)$$

III. RESULTS

A. ggg Enhancements

1. Baryon Enhancements

Figure 3 presents our Λ enhancements binned according to scaled momentum, that is the momentum of the particle divided by the beam energy. In the figure, blue square (green triangle, red diamond) symbols correspond to enhancements on the 1S (2S, 3S) resonance. Closed symbols are data and open symbols are JETSET 7.4[18] event generator simulations followed by the full CLEOIII GEANT-based[19] Monte Carlo detector simulation. We note that the acceptance in the lowest momentum bin is very sensitive to absorption of protons in beam-pipe.

Figure 4 shows the proton and antiproton enhancements. The consistency between the two indicates that beam-wall and beam-gas backgrounds are not substantial.

2. ϕ and $f_2(1270)$ Enhancements

Figure 5 shows ϕ enhancement results binned according to scaled momentum. Symbols are as above with blue square (green triangle, red diamond) symbols correspond to enhance-

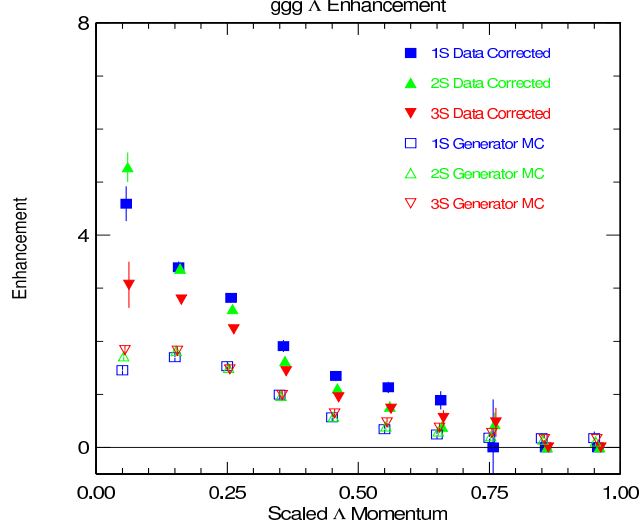


FIG. 3: Raw enhancements for $ggg \rightarrow \Lambda + X$ binned according to scaled momentum (p_Λ/E_{beam}). Blue square (green triangle, red diamond) symbols correspond to enhancements on the 1S (2S, 3S) resonance. Closed symbols are data, open symbols are JETSET Monte Carlo.

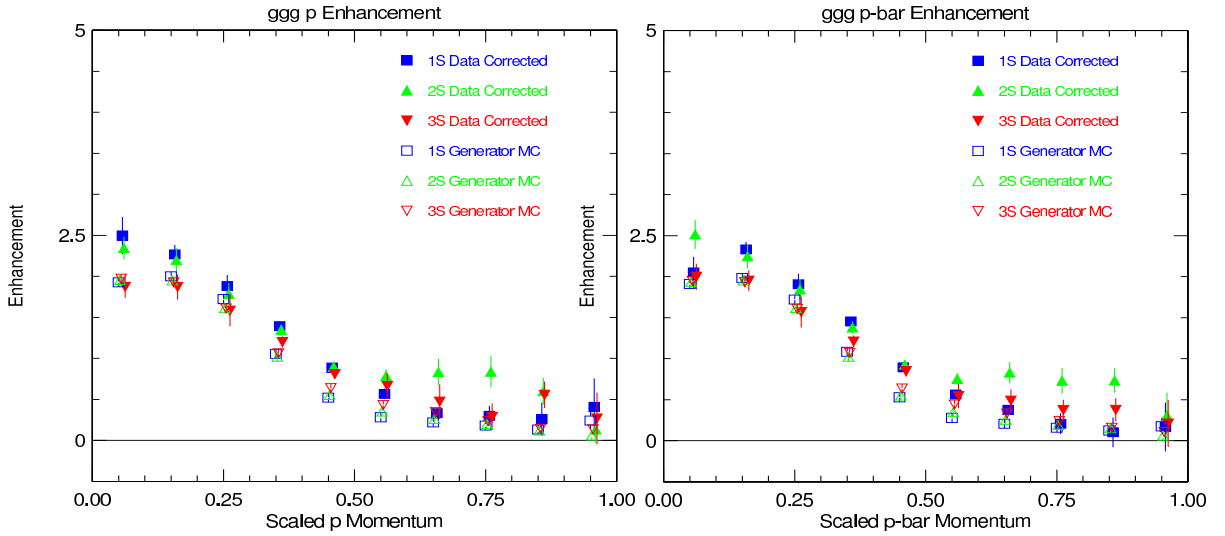


FIG. 4: (Left) Raw enhancements for $ggg \rightarrow p + X$ binned according to scaled momentum. Statistics of continuum subtraction are largest in lower momentum bins. Blue square (green triangle, red diamond) symbols correspond to enhancements on the 1S (2S, 3S) resonance. Closed symbols are data, open symbols are JETSET Monte Carlo. (Right) Same for antiprotons.

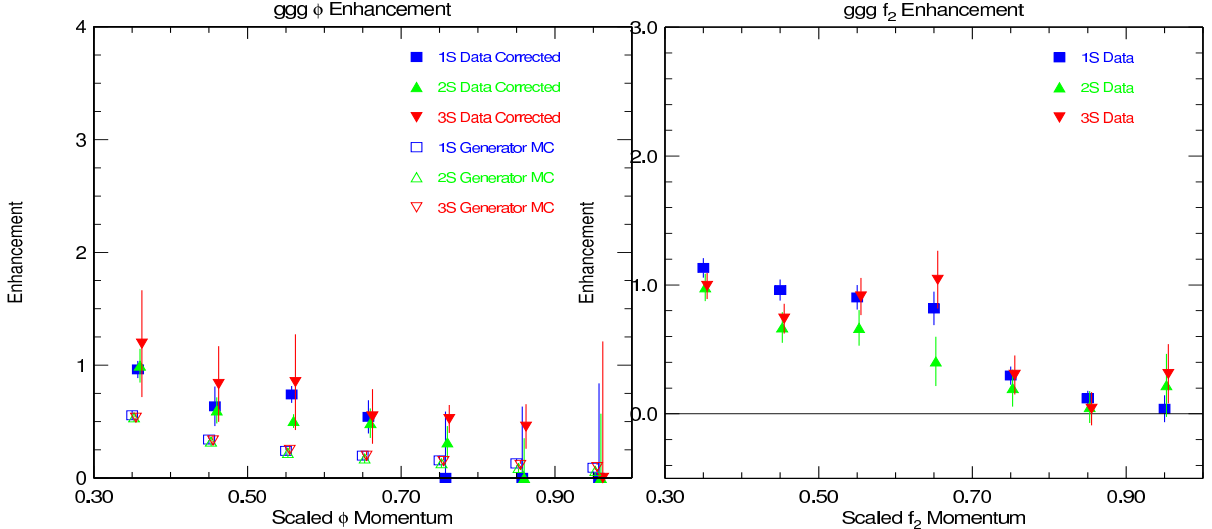


FIG. 5: (Left) Raw enhancements for $ggg \phi$ binned according to scaled momentum. Blue square (green triangle, red diamond) symbols correspond to enhancements on the 1S (2S, 3S) resonance. Closed symbols are data, open symbols are JETSET Monte Carlo. (Right) Enhancements for $f_2(1270)$.

ments on the 1S (2S, 3S) resonance. Closed symbols are data and open symbols are JETSET Monte Carlo. Here, we have normalized the resonant production at 9.46 GeV to the continuum production at 10.55 GeV. Therefore, for ϕ production, the lowest momentum bins for the resonance are particularly sensitive to low-momentum kaon acceptance. Figure 5 also shows the f_2 enhancement results binned according to scaled momentum. The f_2 peak is not well-defined at low momentum (lowest two bins). No Monte Carlo comparison is presented since our current Monte Carlo, by default, will not generate tensor particles.

3. Particle Momentum-Integrated Enhancements

Figure 6 shows the particle momentum-integrated enhancements for each particle. We note that the baryons (Λ , p , \bar{p}) have enhancements greater than 1, while the mesons (ϕ , f_2) have enhancements less than 1. Our results are, in general, numerically consistent with the prior CLEO-I analysis, albeit with considerably higher statistics.

B. $gg\gamma$ Enhancements

There are sufficient statistics to present binned enhancements (in this case binning is done according to tagged photon momentum, not according to individual particle momentum) for Λ , protons and \bar{p} . For all particles, we also present momentum-integrated enhancements.

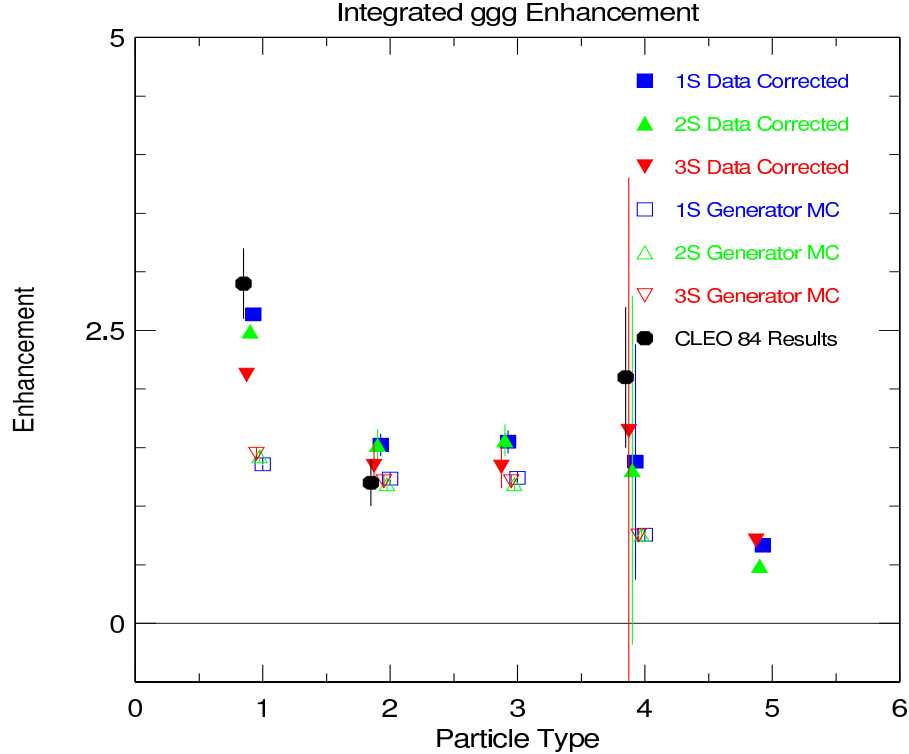


FIG. 6: Compilation of momentum-integrated enhancements for ggg events. Blue square (green triangle, red diamond) symbols correspond to enhancements on the 1S (2S, 3S) resonance. Closed symbols are data, open symbols are JETSET Monte Carlo. The x-axis is arbitrary, chosen to display all particles on one plot: Λ is plotted at $x=1$, protons at $x=2$, \bar{p} at $x=3$, ϕ at $x=4$, and f_2 at $x=5$. Systematic errors and relative efficiencies have now been included for this compilation. The CLEO84 study did not measure an enhancement for $f_2(1270)$ and also only presented a single enhancement for the sum of protons and antiprotons.

1. Baryon Enhancements

Figure 7 shows Λ results binned according to scaled photon momentum, with the color scheme as before. Errors are large in the highest bin due to limited statistics.

Figure 8 shows proton and antiproton enhancement results binned according to scaled photon momentum. We immediately note somewhat smaller enhancements compared to the 3-gluon enhancements presented previously.

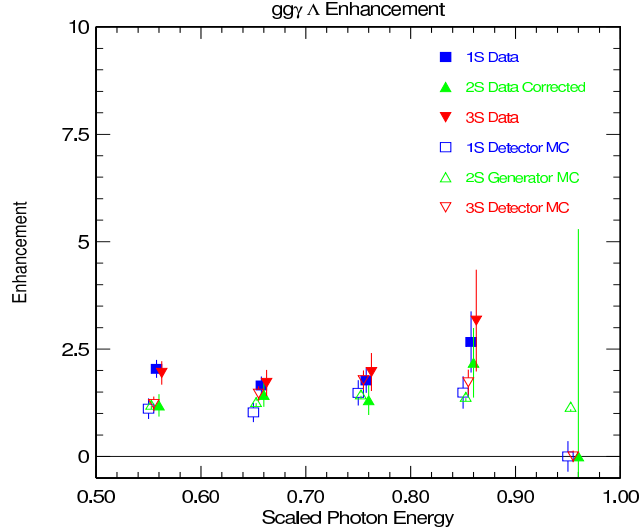


FIG. 7: Raw enhancements for $gg\gamma \rightarrow \Lambda + X$ binned according to scaled photon momentum. We have integrated over all Λ momenta to make these plots, in events having a photon with the indicated x-value. Blue square (green triangle, red diamond) symbols correspond to enhancements on the 1S (2S, 3S) resonance. Closed symbols are data, open symbols are JETSET Monte Carlo.

2. Momentum-Integrated Enhancements

Figure 9 shows the momentum-integrated enhancements for each particle. We note that the enhancements are considerably mitigated in comparison with the case of three-gluon fragmentation.

IV. $\chi_{b,J} \rightarrow \mathbf{P} + \mathbf{X}$

Photon transitions of the $\Upsilon(2S)$ and $\Upsilon(3S)$ to the χ_b states allow us to measure the baryon yields, in association with a radiative transition photon ‘tag’. Typical photon tag energies in this case are of order 80-160 MeV. Due to the large background in this region and therefore limited statistical power, the data permit only an extraction of the proton and antiproton enhancements. Of particular interest is the proton yield in $\chi_{b,2}$ vs. $\chi_{b,1}$ decays; the former is expected to be dominated by decays via two-gluons, the latter is expected to be dominated by decays to $q\bar{q}(g)$, with the gluon expected to carry away very little momentum.

We first conduct a Monte Carlo study to determine the relative efficiency of reconstructing a J=2 transition photon relative to J=1 event, and also the efficiency when we require that a proton be found in addition to the transition photon. We compile statistics on the $\chi_b(\prime) \rightarrow p(\bar{p}) + X$ analyses, separately for J=0/J=1 and for J=2/J=1. For the latter, we fit the signal to a double Gaussian, so that the errors in the areas of the two peaks are correlated and the statistical significance of the signals enhanced. For the former, we simply fit two Gaussians directly. We find that the efficiency for reconstructing a photon-proton

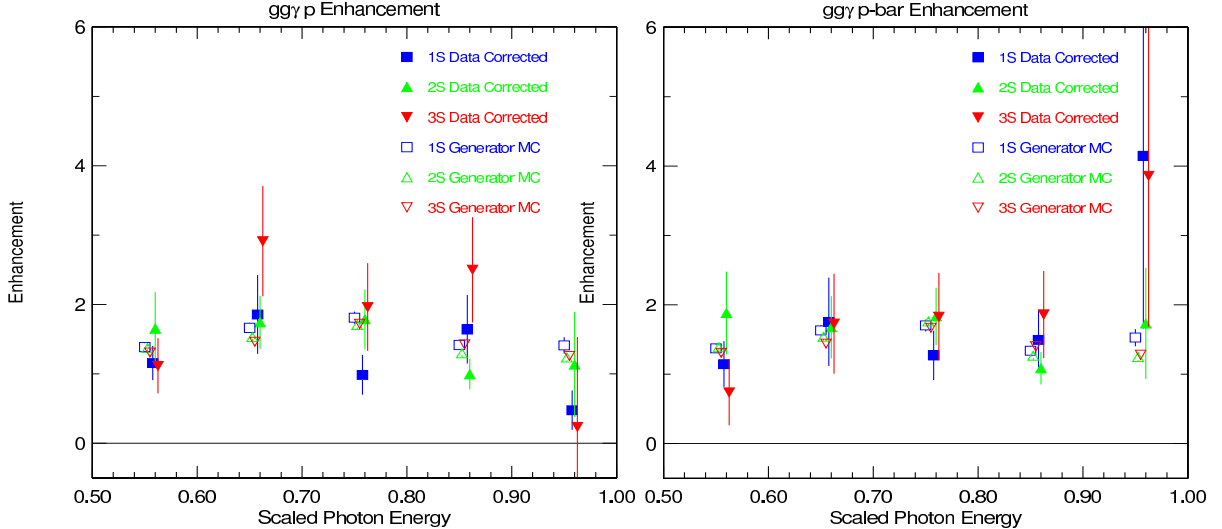


FIG. 8: (Left) Raw enhancements for $gg\gamma p$ binned according to photon momentum. We have integrated over all proton momenta to make these plots, in events having a photon with the indicated x-value. Blue square (green triangle, red diamond) symbols correspond to enhancements on the 1S (2S, 3S) resonance. Closed symbols are data, open symbols are JETSET Monte Carlo. (Right) Same for antiprotons.

correlation in a two-gluon decay is approximately 95% that for a photon-proton correlation in $q\bar{q}(g)$ event.

To check the sensitivity to our particle identification criteria, we have compared results using very tight proton identification requirements (with a reduction in efficiency by more than 50%) vs. the 'standard' loose proton identification criteria used above. We obtain a comparable correction factor using more restrictive particle identification criteria.

Results are presented in the Table II. We note that the observed enhancements are, again, smaller than those observed in comparing three-gluon fragmentation from the Υ resonance with $q\bar{q}$ fragmentation.

V. CROSS-CHECKS AND SYSTEMATICS

In order to verify our procedures and probe possible systematic uncertainties, two primary cross-checks were employed. We first compare the Monte Carlo enhancements at the event generator-level with those determined after the generated events are processed through the full CLEO-III detector simulation ("detector-level"), as a function of momentum. In general, these enhancements will vary for several reasons, including differences in: a) the efficiencies for finding recoil particles in $q\bar{q}\gamma$ vs. $gg\gamma$ events resulting from angular distribution, event multiplicity, and particle momentum differences, b) event selection efficiencies, c) π^0 contamination levels, and d) recoil center-of-mass discrepancies, e.g., between the continuum data under the $\Upsilon(1S)$ resonance vs. the below- $\Upsilon(4S)$ continuum. In cases where the

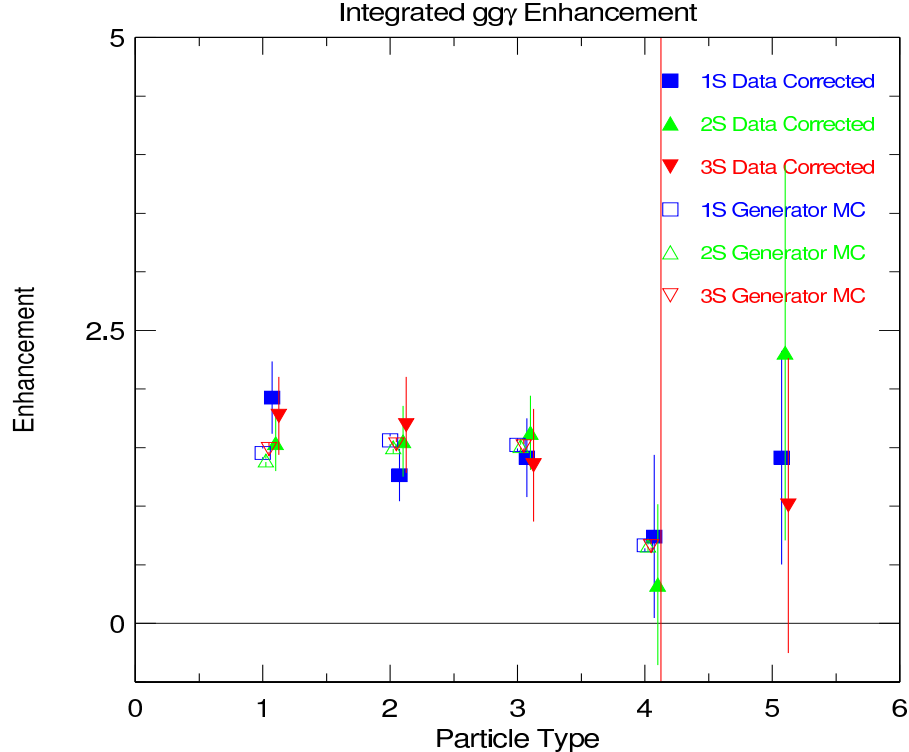


FIG. 9: Momentum-integrated enhancements for $gg\gamma$. Blue square (green triangle, red diamond) symbols correspond to enhancements on the 1S (2S, 3S) resonance. Closed symbols are data, open symbols are JETSET Monte Carlo. The x-axis is arbitrary, chosen to display all particles on one plot: Λ is plotted at $x=1$, p at $x=2$, \bar{p} at $x=3$, ϕ at $x=4$, and f_2 at $x=5$. Systematic errors have been included and relative efficiency corrections have been applied.

generator-level and detector-level enhancements are statistically inconsistent with each other at the 2σ level, we use the ratio between the generator-level and detector-level enhancements as a correction factor and conservatively take half of the amount by which this correction deviates from unity as an estimated systematic error. (Note that these corrections have already been incorporated into the results presented in Figures 6 and 9). Figures 10 and 11 show the comparison of proton enhancements determined at the event-generator vs. post-detector-simulation levels of Monte Carlo simulation. Integrated over momentum, typical corrections are typically of order 10%.

To test the sensitivity of our analysis procedures across different running periods, we have calculated the enhancements for photon-tagged $\Upsilon(4S)$ on-resonance events vs. photon-tagged below- $\Upsilon(4S)$ continuum events, spanning the full CLEO-III data set. Since $\Upsilon(4S) \rightarrow B\bar{B} \sim 100\%$, we expect that any event having a photon with $x_\gamma > 0.5$ is a continuum event. Hence, the calculated enhancement should be zero. In all cases, save for antiprotons, we find good agreement between the below- $4S$ continuum particle yields per photon

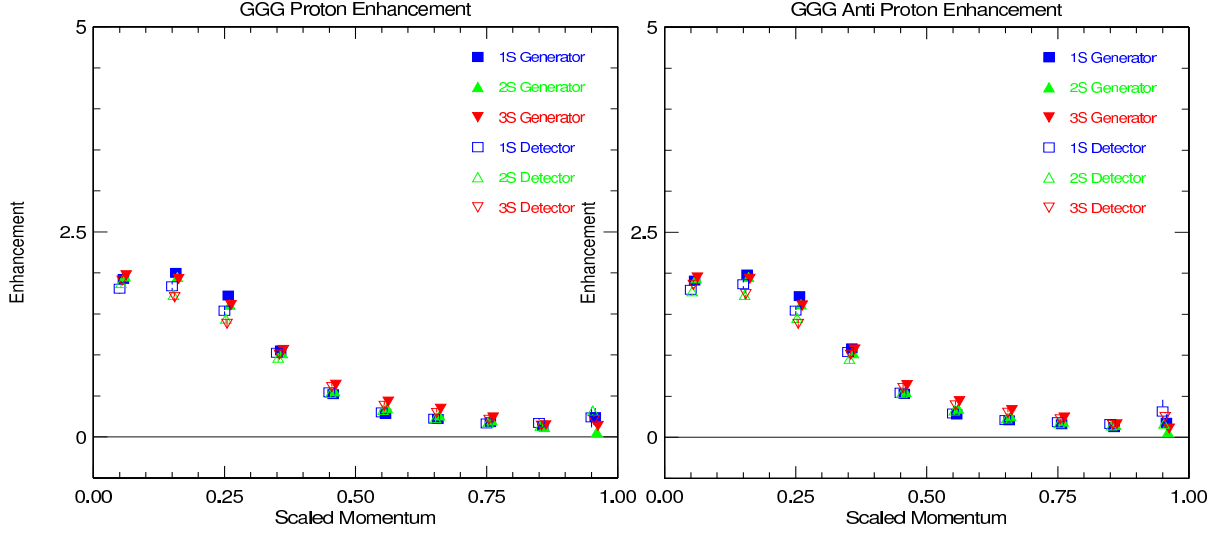


FIG. 10: (Left) Scaled momentum binned enhancements for $ggg \rightarrow p + X$. Blue square (green triangle, red diamond) symbols correspond to enhancements on the 1S (2S, 3S) resonance. Closed (open) symbols are generator (detector) level Monte Carlo enhancements. (Right) Same for antiprotons.

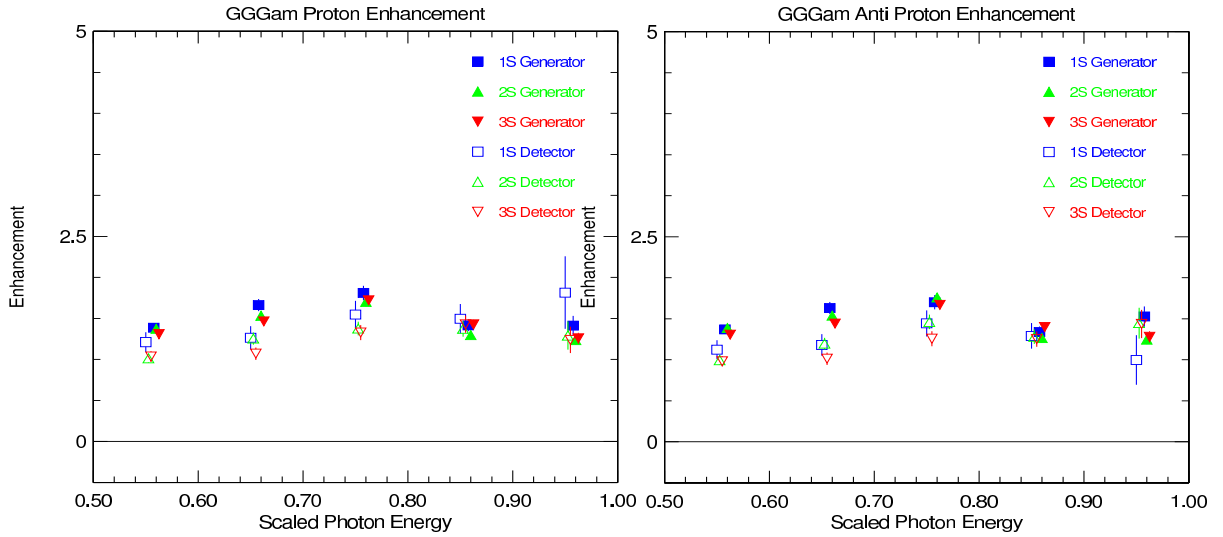


FIG. 11: (Left) Scaled momentum binned enhancements for $gg\gamma$ decays to p . Blue square (green triangle, red diamond) symbols correspond to enhancements on the 1S (2S, 3S) resonance. Closed (open) symbols are generator (detector) level Monte Carlo enhancements. (Right) Same for antiprotons.

TABLE II: Summary of inclusive proton (and antiproton) results for $\chi_{b,J}$ decays. For checks of internal consistency, data have been separated into sub-samples, labeled with capital Roman letters. For J=2 relative to J=1, e.g., the scale of systematic uncertainties is set by the constancy of the value across datasets (r.m.s. \sim 0.03), the magnitude of relative efficiency corrections (\sim 0.05) and the consistency of results obtained using different particle identification criteria.

Dataset	particle Identification	$(J = 2 \rightarrow p + X) / (J = 1 \rightarrow p + X)$	$(J = 0 \rightarrow p + X) / (J = 1 \rightarrow p + X)$
(3S A)	loose	1.116 ± 0.017	1.19 ± 0.046
(3S B)	loose	1.080 ± 0.016	1.00 ± 0.034
(3S C)	loose	1.086 ± 0.011	1.054 ± 0.047
(3S D)	tight	1.103 ± 0.027	1.091 ± 0.097
3S, all		$1.11 \pm 0.01 \pm 0.04$	$1.092 \pm 0.03 \pm 0.06$
(2S A)	tight	1.066 ± 0.028	1.03 ± 0.13
(2S B)	loose	1.075 ± 0.018	1.36 ± 0.15
(2S C)	loose	1.076 ± 0.017	0.99 ± 0.11
(2S D)	loose	1.065 ± 0.015	1.06 ± 0.11
(2S B)	tight	1.076 ± 0.047	1.39 ± 0.28
(2S C)	tight	1.039 ± 0.040	1.17 ± 0.22
(2S D)	tight	1.024 ± 0.035	0.88 ± 0.20
2S, all		$1.068 \pm 0.010 \pm 0.04$	$1.11 \pm 0.15 \pm 0.20$
Monte Carlo (3S A)	loose	1.057 ± 0.016	1.030 ± 0.072
Monte Carlo (3S A)	tight	1.034 ± 0.015	1.042 ± 0.066
Monte Carlo (3S B)	tight	1.041 ± 0.013	1.051 ± 0.049
MC, 3S all		1.043 ± 0.01	1.043 ± 0.036
Monte Carlo (2S A)	tight	1.052 ± 0.014	1.121 ± 0.058
Monte Carlo (2S A)	loose	1.043 ± 0.015	1.076 ± 0.061
MC, 2S all		1.046 ± 0.01	1.061 ± 0.025

tag, and the on-4S particle yields per photon tag. For antiprotons, we find deviations from the null expectation at the level of $\approx 10\%$, and incorporate these deviations (bin-by-bin in momentum) into our total systematic error for that particular case.

VI. DISCUSSION AND SUMMARY

We compare, for the first time, particle production in two-gluon vs. quark-antiquark fragmentation. We find that, in particular, baryon production (per event) in two-gluon decays is somewhat smaller than that observed in three-gluon decays, particularly in the case of Λ production. This result is qualitatively at variance with the conclusion that, e.g., the thrust and charged multiplicity distributions of $\chi_{b,0}$ and $\chi_{b,2}$ two-gluon decays agreed well with $\Upsilon(1S) \rightarrow ggg$ and that the thrust and charged multiplicity distribution of $\chi_{b,1} \rightarrow q\bar{q}g$ agreed with continuum $e^+e^- \rightarrow q\bar{q}$ events[20]. This effect is not reproduced in the current JETSET 7.4 Monte Carlo event generator. For protons, which represent our highest-statistics sample, our results are inconsistent with a model where baryon production in gluon fragmentation is only a function of the available center-of-mass energy. Further detailed

comparisons with models based on either string or independent parton fragmentation may help clarify the production mechanisms.

VII. ACKNOWLEDGMENTS

We gratefully acknowledge the effort of the CESR staff in providing us with excellent luminosity and running conditions. D. Cronin-Hennessy and A. Ryd thank the A.P. Sloan Foundation. This work was supported by the National Science Foundation, the U.S. Department of Energy, and the Natural Sciences and Engineering Research Council of Canada.

-
- [1] S. J. Brodsky and J. Gunion, *Phys. Rev. Lett.* **37**, 402 (1976); K. Konishi, M. Massoth, A. Ukawa and G. Veneziano, *Phys. Lett. B* **78**, 243 (1978).
- [2] H. Kang *et al.* (SLD Collaboration), *Int. J. Mod. Phys.* **A16S1A**, 226 (2001).
- [3] G. Abbiendi *et al.* (OPAL Collaboration), *Eur. Phys. J.* **C37**, 25 (2004).
- [4] G. Abbiendi *et al.* (OPAL Collaboration), *Eur. Phys. J.* **C13**, 1 (2000).
- [5] R. Barate *et al.* (ALEPH Collaboration), *Phys. Lett.* **B434**, 437 (1998).
- [6] P. Abreu *et al.* (DELPHI Collaboration), *Phys. Lett.* **B405**, 202 (1997).
- [7] K. Ackerstaff *et al.* (OPAL Collaboration), *Eur. Phys. J.* **C8**, 241 (1999).
- [8] S. Behrends *et al.* (CLEO Collaboration), *Phys. Rev.* **D31**, 2161 (1985).
- [9] Mike Watkins, Ph. D. thesis, Carnegie-Mellon University, unpublished (2006).
- [10] Gocha analysis, unpublished, hopefully to be submitted to this conference.
- [11] R. A. Briere *et al.* (CLEO Collaboration), *Phys. Rev.* **D70**, 072001 (2004).
- [12] R. A. Briere *et al.* (CLEO Collaboration), submitted to *Phys. Rev. D*.
- [13] M. Artuso *et al.* (CLEO Collaboration), *Phys. Rev.* **D67**, 052003 (2003).
- [14] D. Peterson *et al.*, *Nucl. Inst. Meth.* **A 478**, 142 (2002).
- [15] M. Artuso *et al.*, *Nucl. Inst. Meth.* **A 502**, 91 (2003).
- [16] See, e.g., F. A. Berends and R. Kleiss, *Nucl. Phys.* **B178**, 141 (1981).
- [17] D. Besson *et al.* (CLEO Collaboration), arXiv:hep-ex/0512061, accepted by *Phys. Rev. D*.
- [18] T. Sjostrand, CERN-TH/7111-93.
- [19] R. Brun *et al.*, GEANT v. 3.14, CERN Report No. CERN CC/EE/84-1 (1987).
- [20] S. Alam *et al.* (CLEO Collaboration), *Phys. Rev.* **D46**, 4822 (1992).